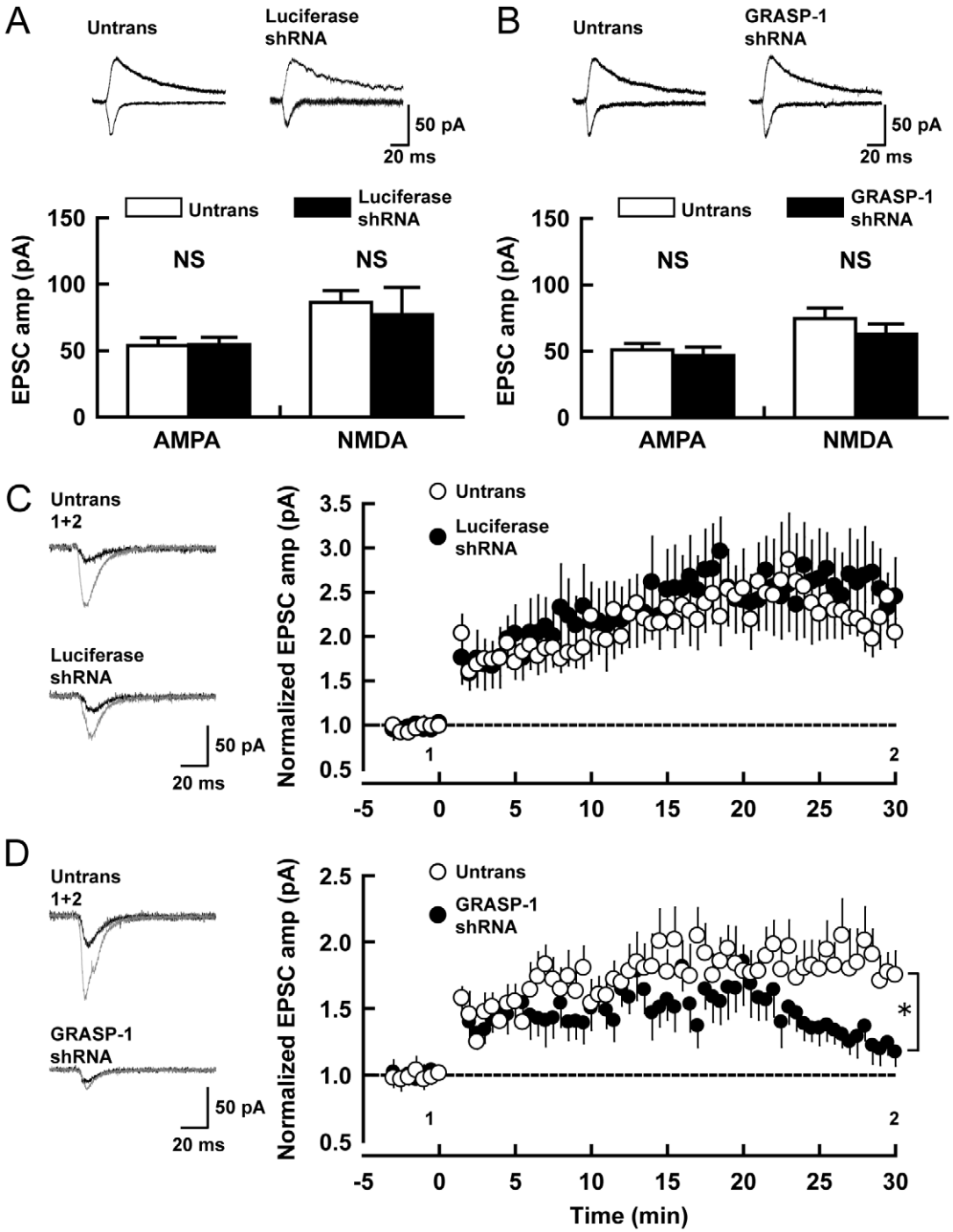

Figure 7. Effect of GRASP-1 knock-down on synaptic transmission and plasticity in hippocampal slice. (A,B) AMPA and NMDA receptor-mediated excitatory synaptic responses were measured from neurons transfected with Luciferase-shRNA (A, control) and GRASP-1-shRNA#5 (B). Top, sample traces mediated by AMPAR (downward) and NMDAR (upward) from pairs of shRNA transfected (Luciferase or GRASP-1-shRNA#5) and neighboring untransfected (Untrans) neurons. Stimulus artifacts were truncated from the traces. Bottom, summary graphs of EPSC amplitudes (AMPA-R-EPSCs and NMDA-R-EPSCs) from shRNA transfected and neighboring untransfected cells. Number of cell pairs: Luciferase-shRNA, 18 and 10; GRASP-1-shRNA#5, 15 and 8 for AMPA and NMDAR-EPSC. NS, not significant. Error bars indicate S.E.M. (C,D) LTP was induced in shRNAs expressing and neighboring untransfected cells by pairing depolarization to 0 mV with 2 Hz stimulation for 100s. Left, sample AMPAR-EPSC traces from untransfected and Luciferase or GRASP-1 shRNA transfected neurons. Currents before (black) and after (gray) are superimposed. Right, time course of AMPA-EPSCs after LTP induction (LTP was induced at $t = 0$). The time points at which sample traces were obtained are indicated by 1 and 2. Number of cell pairs: Luciferase-shRNA, 6; GRASP-1-shRNA#5, 8. * $p < 0.05$.
doi:10.1371/journal.pbio.1000283.g007

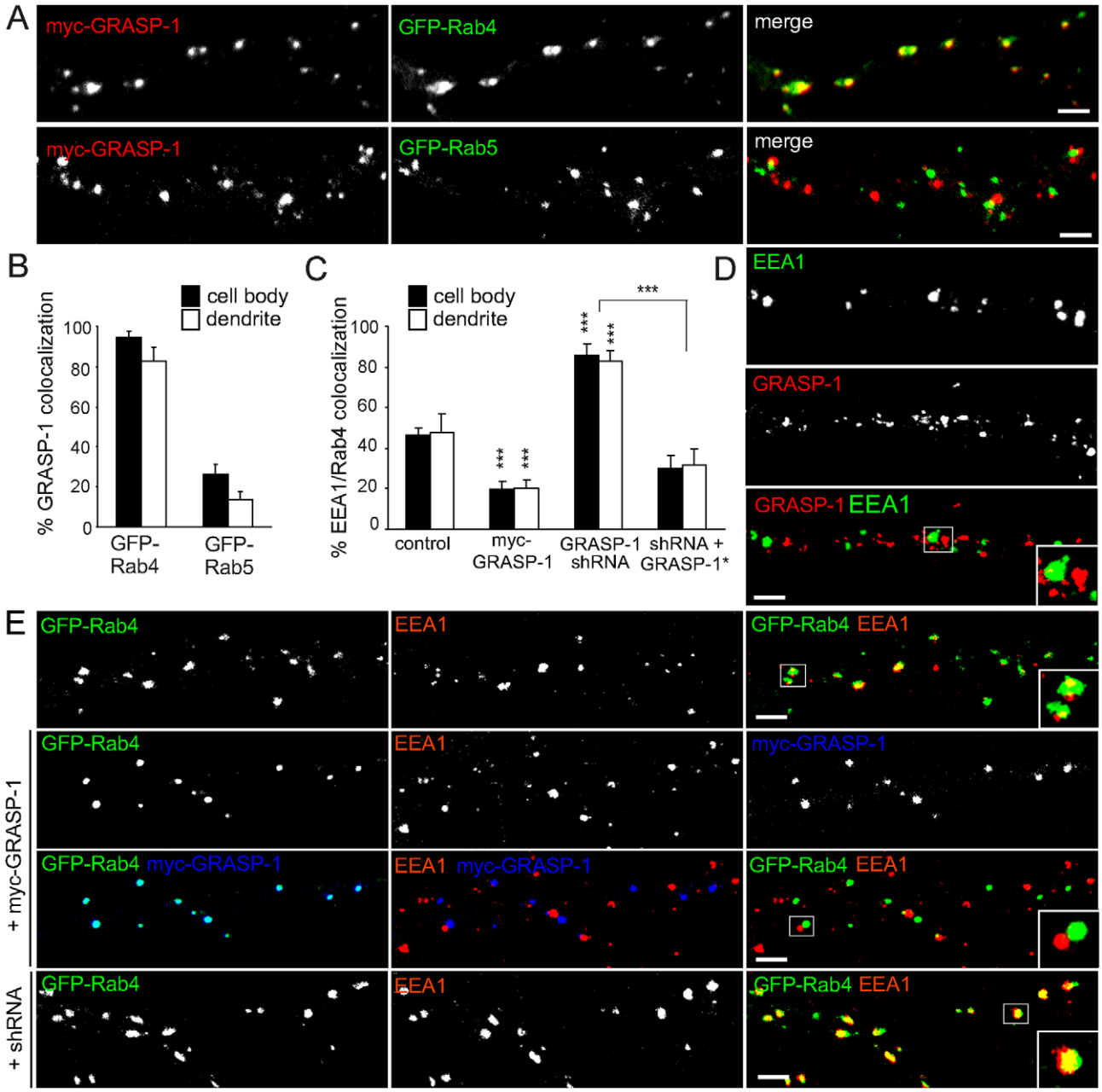

Figure 8. GRASP-1 segregates Rab4 from EEA1 positive endosomal membranes. (A) Representative images of dendrites of hippocampal neurons cotransfected at DIV13 for 4 d with myc-GRASP-1 (red) and either GFP-Rab4 (upper row) or GFP-Rab5 (bottom row). (B) Percentage of colocalization between myc-GRASP-1 and Rab proteins in neurons as indicated in (A). (C) Percentage of Rab4 and EEA1 colocalization in cell body and dendrites as indicated in (E). Error bars indicate S.E.M. *** $p<0.0005$. (D) Representative images of dendrites of hippocampal neurons double-labeled with anti-GRASP-1 (red) and anti-EEA1 (green) antibodies. (E) Representative images of dendrites of hippocampal neurons cotransfected at DIV13 for 4 d with GFP-Rab4 and pSuper control vector, myc-GRASP-1, or pSuper-GRASP-1-shRNA#2 and labeled with anti-EEA1 (red) and anti-myc (blue) antibodies. Bar is 1 μm.
doi:10.1371/journal.pbio.1000283.g008

absence of GRASP-1 we observed a significant decreased Rab4/Rab11 colocalization (15%), compared to control neurons (30% Rab4/Rab11 colocalization), while transfected myc-GRASP-1 robustly enhanced the coalescence of Rab4 and Rab11 domains (80% Rab4/Rab11 colocalization) (Figure 9D,F). Importantly, the observed decrease in EEA1/Rab4 and Neep21/Rab4 domain coupling after myc-GRASP-1 transfection (Figure 8C,E) is consistent with an increase in Rab4/Rab11 domain coupling, while the reverse occurred after GRASP-1 knock-down. These data therefore show that GRASP-1 is a positive regulator of endosomal recycling membrane maturation, via coupling of Rab4- and Rab11-positive endosomal domains.

Syntaxin 13 Binds to GRASP-1 and Connects Recycling Endosomal Domains

GRASP-1 colocalized with endogenous Rab11 (Figure S6) and GFP-Rab11 (Figure 9A) in neurons but did not directly bind to Rab11 (Figure 1C). These observations suggest a crosstalk between

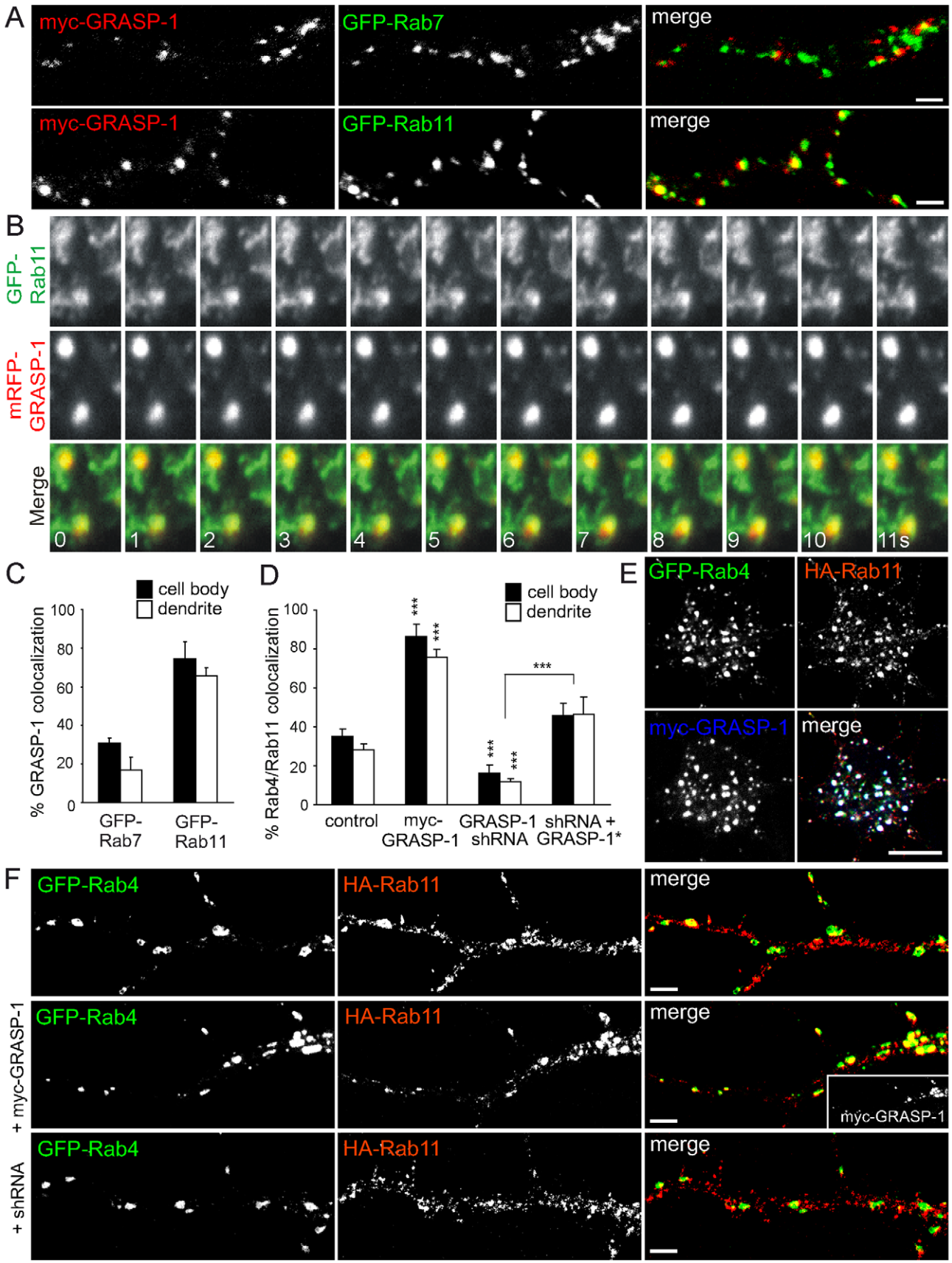

Figure 9. GRASP-1 couples Rab4 and Rab11 domains. (A) Representative images of dendrites of hippocampal neurons cotransfected at DIV13 for 4 d with myc-GRASP-1 and either GFP-tagged Rab7 or Rab11 and labeled with anti-myc (red). Bar is 1 μm. (B) Simultaneous imaging of GFP-Rab11 (green) and mRFP-GRASP-1 (red) in transfected hippocampal neurons. Successive frames are shown and time (seconds) is indicated in the merge

panel. (C) Percentage of colocalization between myc-GRASP-1 and Rab proteins in neurons as indicated in (A). Error bars indicate S.E.M. *** $p<0.0005$. (D) Percentage of colocalization between Rab4 and Rab11 domains in neurons co-transfected with GFP-Rab4 and HA-Rab11 with either myc-GRASP-1, pSuper-GRASP-1-shRNA#2, or pSuper-GRASP-1-shRNA#2 and GFP-GRASP-1* as indicated in (F). (E) Images of cell body of hippocampal neurons triple transfected at DIV13 for 4 d with GFP-Rab4, HA-Rab11, and myc-GRASP-1 and labeled with anti-HA (red) or anti-myc (blue) antibodies. Bar is 10 μm. (F) Representative images of dendrites of hippocampal neurons cotransfected at DIV13 for 4 d with GFP-Rab4 and HA-Rab11 and pSuper control vector, myc-GRASP-1, or pSuper-GRASP-1-shRNA#2 and labeled with anti-HA (red) or anti-myc (inset) antibodies. Bar is 1 μm.
doi:10.1371/journal.pbio.1000283.g009

GRASP-1 and other proteins on Rab11 endosomal domains in hippocampal neurons. One of these candidate proteins is the SNARE syntaxin 13, a transmembrane domain protein that localizes to Rab11 positive tubular recycling endosomes [34,35] and is important for AMPAR recycling, spine morphology, and endosomal mobility [2,12]. We investigated the possible interaction between GRASP-1 and syntaxin 13 by co-immunoprecipitation experiments from COS-7 cells transfected with GFP-GRASP-1 and different myc-syntaxin constructs. GFP-GRASP-1 precipitated syntaxin 13 and not myc-syntaxin 1 and myc-syntaxin 2 (Figure 10A). Consistent, GRASP-1 colocalized with syntaxin 13 (Figures 11A,B and S9) and not with syntaxin 1 (Figure S9A and unpublished data). Moreover, overexpression of GRASP-1 strongly accumulates syntaxin 13 in GRASP-1/Rab4/Rab11 positive structures in neurons (Figure 11A) and Hela cells (Figure S9B). Immunogold EM of neurons showed that syntaxin 13 colocalized with GRASP-1 (Figure 4B) and with Rab4 (Figure 4C) on endosomal tubulovesicular recycling structures, reminiscent of the Rab4-GRASP-1 organelles (Figure 4A). Triple label immuno EM of endogenous Rab4, GRASP-1, and syntaxin 13 indeed revealed partial co-distribution to the endosomal tubulovesicular recycling structures (Figure 4D). This suggests that the three proteins might be

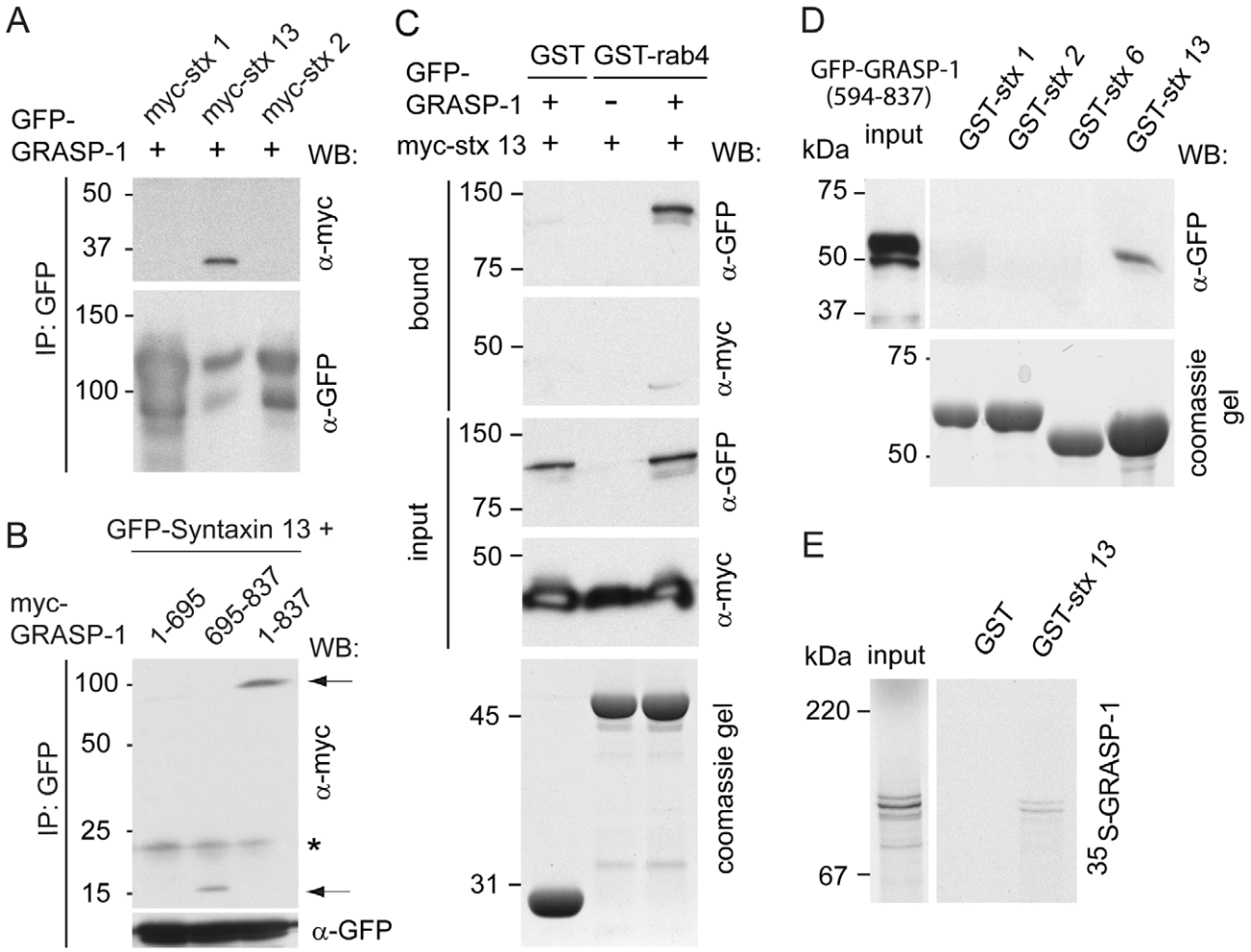

Figure 10. Syntaxin 13 interacts with the C-terminal domain of GRASP-1. (A) Lysates of COS-7 cells cotransfected with GFP-GRASP-1 and myc-syntaxins were immunoprecipitated with anti-GFP antibody and analyzed by Western blot. (B) Lysates of COS-7 cells cotransfected with GFP-syntaxin 13 and full-length myc-GRASP-1 (1–837) or truncated myc-GRASP-1 constructs (1–695 or 695–837) were immunoprecipitated with anti-GFP antibody and analyzed by Western blot. Asterisk indicates background band. Arrows point to co-precipitated GRASP-1 proteins. (C) Binding assay using lysates of COS-7 cells expressing myc-syntaxin 13 with or without GFP-GRASP-1 and GMP-PNP-charged GST-rab4. Note that myc-syntaxin 13 is only isolated on the beads in the presence of GRASP-1. (D) Binding assay using lysate of COS-7 cells transfected with GFP-GRASP-1(594–837) and GST-syntaxins without transmembrane domain (ΔTM). GRASP-1 was analyzed by Western blot with antibody against GFP. (E) Binding assay of ^{35}S-labeled GRASP-1 and immobilized GST-syntaxin 13ΔTM.
doi:10.1371/journal.pbio.1000283.g010

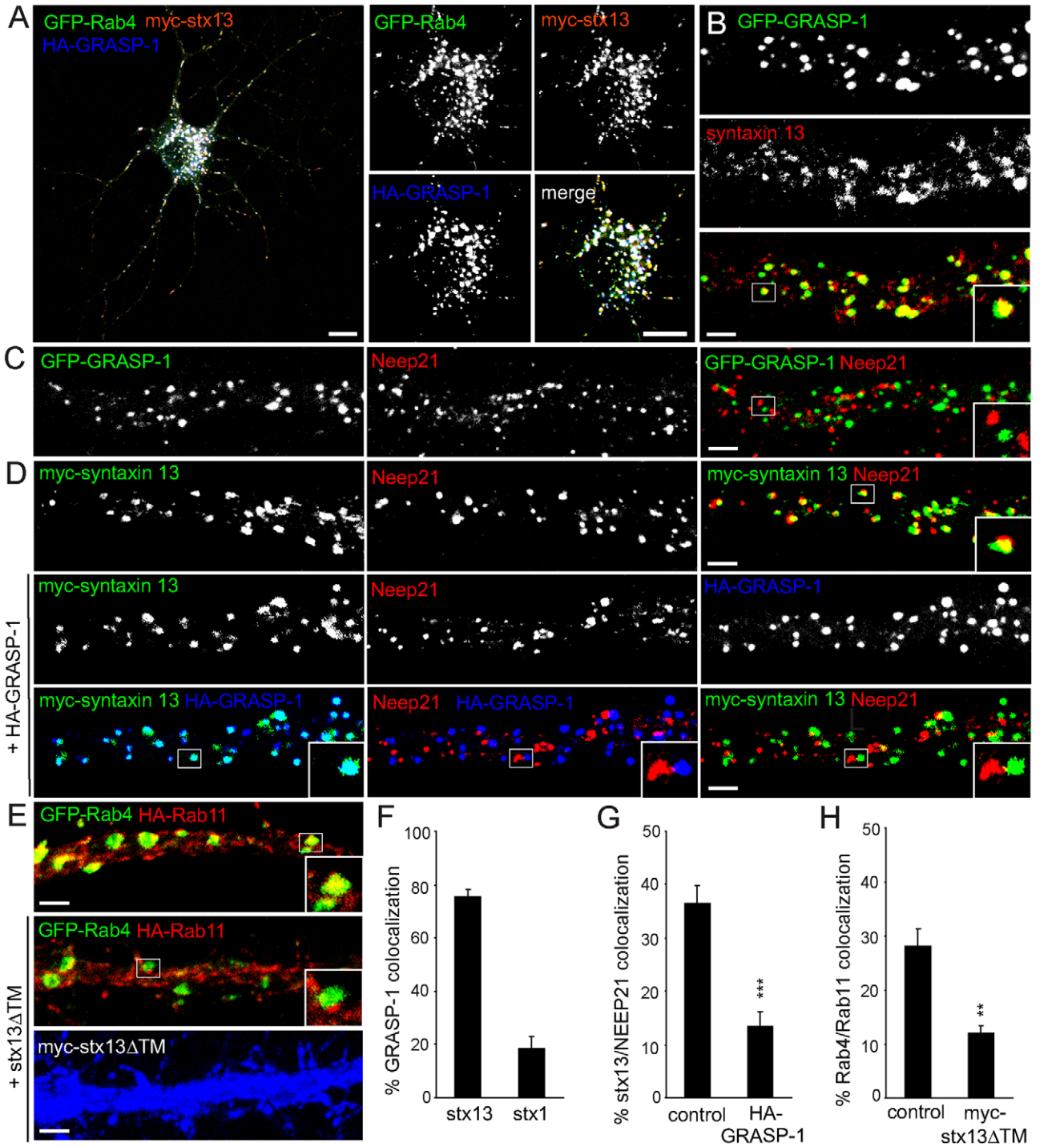

Figure 11. Syntaxin 13 coincides with GRASP-1 and segregates Rab4/Rab11 domains. (A) Representative image of hippocampal neuron triple transfected at DIV13 for 4 d with GFP-Rab4, HA-GRASP-1, and myc-syntaxin 13 and labeled with anti-HA (blue) or anti-myc (red) antibodies. Magnified region of the cell body is shown to indicate the strong colocalization of GRASP-1, Rab4, and syntaxin 13. (B) Representative images of dendrites of hippocampal neurons transfected at DIV13 with GFP-GRASP-1 for 4 d and labeled with anti-syntaxin 13 (red). (C) Representative images of dendrites of hippocampal neurons transfected at DIV13 with GFP-GRASP-1 for 4 d and labeled with anti-Neep21 (red). (D) Representative images of dendrites of hippocampal neurons cotransfected at DIV13 for 4 d with myc-syntaxin 13 and control vector or HA-GRASP-1 and labeled with anti-myc (green), anti-HA (blue), and anti-Neep21 (red). (E) Representative images of dendrites of hippocampal neurons cotransfected at DIV13 for 4 d with GFP-Rab4, HA-Rab11, and control vector or myc-syntaxin 13ΔTM and labeled with anti-myc (blue) and anti-HA (red). (F) Percentage of colocalization between HA-GRASP-1 and myc-syntaxin 1 or myc-syntaxin 13 in neurons. (G) Percentage of colocalization between myc-syntaxin 13 and Neep21 in dendrites as indicated in (D). (H) Percentage of colocalization between GFP-Rab4 and HA-Rab11 domains in dendrites expressing myc-syntaxin 13ΔTM as indicated in (E). Error bars indicate S.E.M. ** $p<0.005$. *** $p<0.0005$. Bar in A is 10 μm; Bar in (B–E) is 1 μm.
doi:10.1371/journal.pbio.1000283.g011

engaged in a complex on endosomal membranes. In agreement with this hypothesis, myc-syntaxin 13 could be isolated from COS-7 lysates on GST-Rab4 beads, only if GRASP-1 was co-transfected (Figure 10C). The interaction required the PDZ-like domain containing C-terminal region of GRASP-1, but not the N-terminal Rab4 binding domain (Figure 10B,D), and could be recapitulated with purified GST-syntaxin 13 and ^{35}S-labeled GRASP-1 (Figure 10E). Since syntaxin 13 has a transmembrane domain, it could be an anchor for GRASP-1 on endosomal membranes. In accord, the C-terminal part of GRASP-1 is necessary for the localization of GRASP-1 to TfR containing endosomes (Figure S10). However, GRASP-C alone is not sufficient for GRASP-1 membrane localization since the Rab4 binding domain is also required (Figure S10).

Previously, syntaxin 13 was found in complexes with early endosomal proteins EEA1 [36] and Neep21 [13]. To better understand the role of syntaxin 13 in both early and recycling endosomes, we first investigated the distribution of syntaxin 13 in dendrites of hippocampal neurons and found ~40% overlap between Neep21 and syntaxin 13 (Figure 11D,F), ~40% colocalization between GRASP-1 and endogenous syntaxin 13 (Figure 11B), while no co-distribution of Neep21 with GRASP-1 was observed (Figure 11C, Figure S6). These data suggest that GRASP-1/syntaxin 13 and Neep21/syntaxin 13 are associated with distinct endosomal structures. Since expression of GFP-GRASP-1 strongly accumulates endogenous syntaxin 13 in the cell body and dendrites without recruiting Neep21 (Figure S6), we examined whether GRASP-1 influences the Neep21/syntaxin 13 complex. Overexpression of GRASP-1 strongly reduced the colocalization between syntaxin 13 and Neep21 (~15%) compared to control neurons (~40%) (Figure 11D,G), suggesting that GRASP-1 competes with Neep21 for binding to syntaxin 13, thereby affecting the integrity of the Neep21/syntaxin 13 complex. These data are consistent with the observation that GRASP-1 separates Rab4 from Neep21 endosomal domains.

To evaluate whether syntaxin 13 is important for GRASP-1 association with Rab11 domains, we triple transfected GFP-Rab4, HA-Rab11, and a myc-tagged dominant negative syntaxin 13ΔTM mutant lacking the transmembrane domain. Hippocampal neurons transfected with syntaxin 13ΔTM showed a strong decrease in Rab4/Rab11 colocalization (~10%) compared to control neurons (~30%) (Figure 11E,H), while the co-distribution of Rab4 and GRASP-1 was not affected (unpublished data). These data indicate that syntaxin 13 regulates Rab4/GRASP-1 association with Rab11 endosomes.

Discussion

Complex processes that govern neuronal function have adapted basic cellular pathways to perform the elaborate information processing achieved by the brain. Some of these processes, such as cargo trafficking, require additional layers of control and fine-tuning. Here, we describe a new molecular mechanism for regulating endosomal membrane and receptor recycling by GRASP-1 in neuronal cells. GRASP-1 is a neuronal effector of Rab4, binds syntaxin 13, and couples Rab4 and Rab11 endosomal domains. This mechanism has two distinct roles in neuronal function; first, it is required for AMPAR recycling, and second, it is critical for dendritic spine morphology.

Regulation of Recycling Endosome Maturation by GRASP-1

Each organelle carries its own set of Rabs which ensures the specificity of intracellular membrane transport. Ample examples show that Rab GTPases and their effectors can confer directionality to membrane traffic and couple different traffic steps [37]. Here, we show that GRASP-1 is a new component of the molecular machinery that regulates directionality in endosomal trafficking in neurons. First, GRASP-1 is a novel Rab4 effector and binds specifically to its active GTP-bound state. Second, knock-down of GRASP-1 separates Rab4 and Rab11 domains and moves Rab4 in EEA1/Neep21 positive early endosomal structures. Accordingly, knock-down of GRASP-1 mimics the effects of dominant-negative Rab4 and Rab11 on dendritic spine morphology. Third, GRASP-1 overexpression strongly increases Rab4/Rab11 colocalization in both neurons and Hela cells. We propose a model in which GRASP-1 coordinates recycling endosomal maturation (Figure 12). The term *recycling endosome maturation* is used here to discern it from the other endosomal exit routes, such as the degradative multivesicular body/endosome

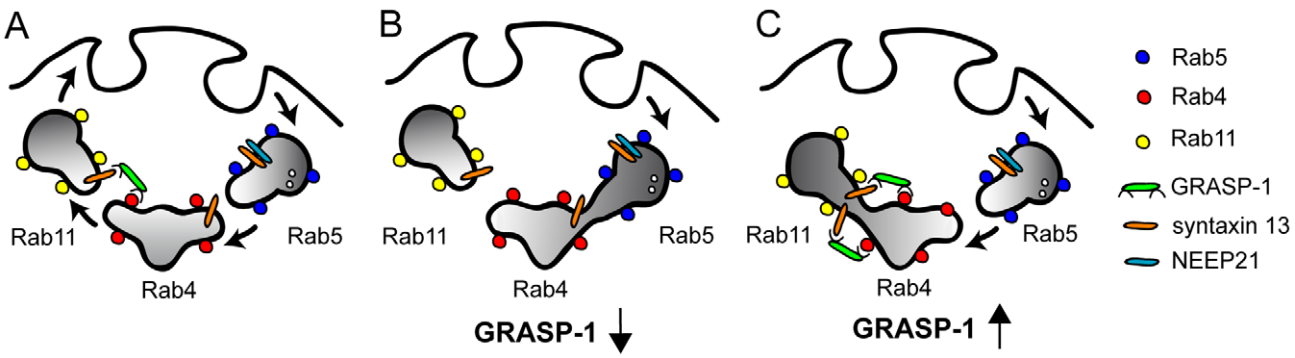

Figure 12. Model for the role of GRASP-1 in endosome recycling. Endosomes can be viewed as mosaic distribution of Rab4, Rab5, and Rab11 domains that dynamically interact via effector proteins and SNAREs. The Rab5 domain allows entry into the early/sorting endosome, whereas the Rab4 and Rab11 domains contain the machinery that is necessary for sorting and recycling membranes and receptors back to the plasma membrane. (A) GRASP-1 binds to Rab4 and syntaxin 13 and couples Rab4 and Rab11 recycling endosomes. The complex formed between GRASP-1 and t-SNARE syntaxin 13 might mediate fusion between Rab4 and Rab11 endosomes. (B) Absence of GRASP-1 interferes with complex formation at the recycling step, causing cargo accumulation in early endosomes, impairment of receptor expression, and changes in spine morphology. (C) Overexpression of GRASP-1 leads to recruitment of syntaxin 13 and strongly couples Rab4 and Rab11 domains, causing accumulation of internalized receptors in recycling endosomes. Consistent with the observed decrease in AMPAR clusters [28], Caspase-3 cleavage of GRASP-1 might separate the N-terminal Rab4 domain from the C-terminal syntaxin 13 binding site and disrupt the coupling between Rab4 and Rab11 domains.
doi:10.1371/journal.pbio.1000283.g012

maturation pathway, the retrieval route of mannose 6-phosphate receptors to the trans Golgi network, or the pathway for melanogenic enzymes to melanosomes [38].

How does GRASP-1 couple specific Rab domains? Along the endosomal pathway, bivalent effectors have been found that connect proximal Rab5 and Rab4 domains on early endosomes [25]. Since GRASP-1 binds directly to Rab4 but not to Rab11, additional factors are needed. We found that GRASP-1 binds to endosomal SNARE protein syntaxin 13. Overexpression of GRASP-1 separates syntaxin 13 from Neep21 positive structures and strongly recruits syntaxin 13 to Rab4 positive membranes. Previous studies have shown that syntaxin 13 is involved in recycling of endosomal domains [13,35] and is enriched in Rab11 endosomal fractions [34]. Syntaxin 13 also has a function together with syntaxin 6 in the fusion of early endosomes in vitro [39,40]. We found that mutant syntaxin 13 separates Rab4/GRASP-1 and Rab11 positive endosomal domains, suggesting a novel function of syntaxin 13 in the coupling of Rab4 and Rab11 domains by GRASP-1. Since syntaxin 13 is a constituent of the SNARE core complex [35] and involved in membrane fusion [36], it is tempting to speculate that the binding between GRASP-1 and syntaxin 13 recruits the fusion machinery necessary to connect with Rab11 positive membranes. Additional studies are required to determine the precise functional relationship between GRASP-1 binding to syntaxin 13 and the SNARE function of syntaxin 13.

The property to bind Rab4 via the N terminus and syntaxin 13 via the C terminus of GRASP-1 supports the model that membrane bound active Rab4 retains or recruits GRASP-1 on endosomes and forms a complex with syntaxin 13. This sequence of interactions could then structurally and functionally link Rab4 to Rab11 membrane domains (Figure 12). Subsequent recruitment of the other factors on to Rab4-defined membrane domains could strengthen the interaction with Rab11. It has been speculated that the GTPase-activating proteins (GAPs) that act on the upstream Rabs might be effectors of the downstream Rabs [41]. These Rab cascades and conversions might serve as a positive feedback loop to specifically concentrate activated Rab4 on Rab11 positive endosomes. Additional regulation of GRASP-1 by caspase-3 cleavage [28] could separate the N-terminal Rab4 binding domain from the C-terminal syntaxin 13 binding site, potentially disrupting the interaction between Rab4 and Rab11 endosomes (Figure 12).

Role of GRASP-1 in Endosomal AMPAR Recycling

GRASP-1 was originally found to act as a neuronal Ras GEF and regulate synaptic AMPAR trafficking [28]. We could not measure detectable GEF activity of GRASP-1 for Ras in vivo, by filter binding (unpublished data) or sensitive fluorometric mantGDP assays, nor did we find homology between the GRASP-1 sequence and known rasGEF domains. Here, we provide an alternative model for the role of GRASP-1 in AMPAR traffic and show that GRASP-1 is part of the molecular machinery that controls endosomal membrane receptor recycling in dendrites. Indeed, we show that GRASP-1 colocalizes with internalized AMPARs and that knock-down of GRASP-1 decreases recycling of GluR subunits after AMPA application. Moreover GRASP-1 regulates synaptic plasticity, especially the late phase of LTP in hippocampal slices. Previous results show that Rab11 and syntaxin 13 dominant negative mutants were critical for the entire time course of LTP [12,22]. We propose that GRASP-1 regulates a particular step in the endosomal trafficking and is important for a specific phase of AMPA receptor recycling (Figure 12). In addition to supplying AMPARs, membrane trafficking from recycling endosomes also mediates the growth of dendritic spines [2,22,42]. In accord, GRASP-1 knock-down decreased the total number of protrusions and mushroom-shaped spines and regulates endosomal mobility into dendritic spines. As discussed above, the coupling of endosomal Rab4 and Rab11 domains by GRASP-1 is an attractive possibility to explain the effects on AMPAR recycling and spine morphology.

GRASP-1 binds to the seven PDZ domain-containing scaffolding protein GRIP [28] that transports and stabilizes GluR2 containing AMPAR at synapses and intracellular compartments [5,43]. Rab4 dominant negative and GRASP-1 knock-down had no effect on GRIP-1 distribution and Rab4/GRASP-1 positive endosomal structures did not recruit endogenous GRIP (unpublished data), suggesting that GRIP functions in an alternative trafficking pathway independent of GRASP-1 or the interaction with GRASP-1 is transient and highly regulated. Interestingly, GRIP also binds to the early endosomal protein Neep21, which is crucial for AMPAR sorting through endosomes [44,45]. Since neuronal activity determines the phosphorylation status of GRIP and enhances the binding of GRIP and GluR2 with Neep21 [44,45], it is possible that GRIP is under tight control of specific phosphorylation signaling mechanisms in order to allow for consecutive protein binding and temporal receptor interactions [44,45]. Additional studies are required to determine the precise role of GRIP in endosomal receptor trafficking.

In contrast to AMPA stimulation, GRASP-1 staining strongly decreased by bath application of NMDA [10,28]. It has been shown that AMPA and NMDA stimulation induce differential AMPAR sorting; AMPA stimulation allows AMPARs to enter the normal recycling pathway, whereas NMDA stimulation diverts AMPARs to Neep21-positive endosomes and the lysosome degradation pathway [10,13]. It is tempting to speculate that GRASP-1 in AMPA stimulated neurons allows sorting of internalized AMPARs to the recycling endosomes, while in response to NMDA, absence of GRASP-1 drives receptors to the lysosomes. It is possible that different neuronal stimulatory inputs dynamically control activity of effector complexes and endosomal trafficking pathways. In this model, GRASP-1 might be part of the machinery on endosomes that senses and reacts on NMDA receptor-mediated Ca^{2+} influx, which is of key importance to understanding internalized AMPAR and membrane sorting during plasticity and neuronal circuitry remodeling.

Materials and Methods

Antibodies and DNA Constructs

The following primary antibodies were used in this study: rabbit anti-GRASP-1 (JH 2730) [28], rabbit anti-NEEP21 [13], rabbit anti-GRIP1 [43], rabbit anti-Rab4 [46], rabbit anti-GFP [47], rabbit anti-syntaxin 13 [35]. Rabbit anti-Rab11 was generated by immunizing animals with GST-Rab11a and affinity purified on His-Rab11a columns. Anti-GRASP-1 (#5285) was generated by immunizing rabbits with GST-GRASP-1(1–378) and used for immuno electronmicroscopy.

The following antibodies were obtained from commercial sources: rabbit anti-GRASP-1 (AB96361), mouse anti-β-actin, mouse anti-GluR2 (Chemicon), mouse anti-Rab4, mouse anti-EEA1 (BD Biosciences), mouse anti-FLAG, mouse anti-MAP2, mouse anti-αtubulin (Sigma), mouse anti-GFP (Roche), mouse anti-bassoon (Stressgen), rabbit anti-β-galactosidase (MP Biomedicals), mouse anti-β-galactosidase (Promega), rabbit anti-GluR1 (Calbiochem), mouse anti-HA (Roche), rabbit anti-myc (Upstate Biotechnology), mouse LAMP-1 (Stressgen), mouse anti-myc, rabbit anti-Rab5 (Santa Cruz Biotechnology), rabbit anti-syntaxin 13 (Synaptic Systems), human anti-EEA1, and mouse anti-human

TfR (ATCC). TfR-594, HRP, and fluorescently labeled secondary antibodies were from Molecular Probes and Jackson Laboratories, and agarose beads conjugated with mouse anti-FLAG antibody were purchased from Sigma. The following mammalian expression plasmids have been described: pRK5-myc-GRASP-1 [28], pEF-Flag-Rab4 and pEF-Flag-Rab5 [48], pEGFP-Rab7 [49], pβactin-HA-β-galactosidase [43], pJPA5-Tfr-GFP [50], Rab3, Rab4, Rab5, Rab7 and Rab11 cDNA in pGEX, pEGFP or pcDNA3 [47,51–54], pGEX-Hras(1–166) and pGEX-cdc25(974–1260) [55], pcDNA3-NEEP21-GFP, pcDNA3-myc-syntaxin 13 [13], pEGFP-Rab11S25N [56], pEGFP-Rab4S22N [57], pGW1-HA-GluR2 [10], pSuper vector [58], and pSuper-GRIP1-shRNA [43]. pMT2HA-rasGRP and pMT2HA-ras were obtained from Hans Bos (Laboratory of Physiological Chemistry, University Medical Center, Utrecht). Syntaxin constructs were obtained as indicated; pGEX-syntaxin1ΔTM and pGEX-syntaxin2ΔTM (Ruud Toonen, CNCR, VU, Amsterdam), pGEX-syntaxin6ΔTM (Suzanne Pfeffer, Stanford School of Medicine), and pGEX-syntaxin13ΔTM (Andrew Peden, CIMR, Cambridge).

GRASP-1 truncation constructs and GRASP-1 mutant lacking aa280–300 were made with PCR from full-length GRASP-1 cDNA 1 [28]. GRASP-1* rescue constructs were prepared by a PCR-based strategy to introduce four silent substitutions in the target site. The target sequence GCTCTCTGAGAAATTGAAA was modified into GCTTTCGGAAAAGTTGAAA. Syntaxin-1A (BC100446; image: 6595634), syntaxin-2 (BC047496; image: 5296500), and syntaxin-6 (BC009944; image: 4122224) cDNA was purchased from Geneservice. For neuronal expression, all cDNAs were subcloned in pGW1- and pβactin-expression vectors with various tags [43]. Myc-syntaxin 13ΔTM (aa1–245) was made by PCR from full-length syntaxin 13 cDNA. The rat GRASP-1 (accession NM_053807) smartpool siRNA (cat# L-096315-01) was from Dharmacon. Another set of three separate siRNAs targeting rat GRASP-1 was purchased from Ambion (cat# AM16798A). GRASP-1-siRNA2 (siRNA ID#192942, GCUCUCUGAGAAA-UUGAAAtt) yielded most efficient knock-down in INS1 cells and was cloned in pSuper plasmid for knock-down of GRASP-1 in rat hippocampal neurons. GRASP-1 shRNA#5 (GTCCCAGCA-CAAAGAAGAA) was designed by using the siRNA selection program at the Whitehead Institute for Biomedical Research [59] (jura.wi.mit.edu/bioc/siRNAext). The sequence for the Luciferase shRNA is CGTACGCGGAATACTTCGA [60].

Preparation of Tissue Extracts

For tissue Western blots, cerebral cortex, cerebellum, midbrain, spinal cord, kidney, liver, and spleen were dissected from P30 mice. Frozen tissue samples and cultured cells were homogenized in PBS/1%Triton-×100, and then an equal volume of 2× SDS sample buffer was added, and the samples were boiled. Protein concentrations were measured using a BCA protein assay kit (Pierce), and 20 μg of protein was loaded in each lane for a subsequent Western blot analysis.

GST-Rab Pull-Down Assays

Preparation of pig brain cytosol, purification of GST-Rab fusion proteins, isolation of Rab4GTP-interacting proteins in pull-down assays and binding assays with ^{35}S-labeled GRASP-1 were done as described [52,61]. To determine the Rab4 binding region on GRASP-1, we expressed pRK5-myc GRASP-1 or pGW1-GFP-GRASP-1 truncations in COS-7 cells. Cells were washed in ice-cold PBS and lysed in 20 mM Hepes pH 7.4, 100 mM NaCl, 5 mM $MgCl_2$ (lysis buffer) containing 0.5% NP-40, 5 μg/ml leupeptin, 10 μg/ml aprotinin, 1 μg/ml pepstatin, 1 mM PMSF, 20 μM GMP-PNP, and 1 mM DTT. Detergent lysates were shaken for 20 min at 4°C, centrifuged for 10 min at maximum speed in a cooled Eppendorf centrifuge, diluted with lysis buffer to 0.2% NP-40, and incubated with Rab4-GMP-PNP beads for 2 h at 4°C. Beads were washed four times with lysis buffer containing 0.2% NP-40, 20 μM GMP-PNP, and 1 mM DTT. Bound proteins were eluted in Laemmli sample buffer and analyzed by Western blot and detection with anti-myc antibody. To determine whether Rab4, GRASP-1, and syntaxin 13 can form a ternary complex, we transfected COS-7 cells with pGW1-myc-syntaxin 13 with and without pGW1-GFP-GRASP-1. Cells were lysed in 20 mM Na Hepes pH 7.5, 100 mM NaCl, 1% TX-100, and cleared detergent lysates were incubated with GST-Rab4 or GST beads. Beads were washed three times with lysis buffer, and bound protein was assayed by Western blot with monoclonal antibodies against GFP and myc epitope tags.

Binding Assays with GST-Syntaxins

GST-syntaxin fusion proteins lacking the transmembrane domain were expressed in *Escherichia coli* BL21(DE3), immobilized on GSH beads, and used for binding assays with lysates of COS-7 cells transfected with GFP-GRASP-1(594–837). Binding assay of GST-syntaxin13ΔTM and ^{35}S-labeled GRASP-1, produced in a coupled in vitro transcription-translation reaction, was done as described [61]. For mapping the syntaxin 13 binding domain on GRASP-1, we expressed C terminal pGW1-GFP-GRASP-1 constructs in COS-7 cells. The cells were metabolically labeled for 30 min with 0.5 mCi/ml ^{35}S-methionine/Pro-Mix (Perkin Elmer), and detergent lysates were then subjected to a GST pull-down assay on GST-syntaxin13ΔTM as described above. Bound proteins were released by boiling the beads 8 min in 0.1 ml 1% SDS/PBS, and GFP-tagged GRASP-1 truncations were immunoprecipitated with a rabbit GFP antibody and analyzed by phosphorimaging as before [62].

Mass Spectrometry

Eluates were boiled in Laemmli sample buffer, resolved on a 7.5% SDS-PAA gel, and silver-stained. Bands of interest were excised and in-gel digested using modified trypsin (Roche Diagnostics, Indianapolis, IN) in 50 mM ammonium bicarbonate. The peptide mixtures were analyzed by LC/MS/MS using a Q-ToF hybrid mass spectrometer (Micromass, Waters) equipped with a Z-spray source and coupled on-line with a capillary chromatography system. The peptide mixtures were delivered to the system using a Famos autosampler (LC Packing) at 3 μl/min and trapped on an AquaTM C18RP column (Phenomenex; column dimension 1 cm×100 μm i.d., packed in house). The sample was then fractionated onto a C_{18} reverse-phase capillary column (PepMap, LC Packing; column dimension 25 cm×75 μm i.d.) at a flow rate of 150–200 nl/min using a linear gradient of acetonitrile. The mass spectrometer was set up in a data-dependent MS/MS mode where a full scan spectrum (m/z acquisition range from 400 to 1,600 Da/e) was followed by a tandem mass spectrum (m/z acquisition range from 100 to 1,800 Da/e). The precursor ions were selected as the most intense peaks of the previous scan. Suitable collision energy was applied depending on the mass and charge of the precursor ion. ProteinLynx software, provided by the manufacturers, was used to analyze raw MS and MS/MS spectra and to generate a peak list which was introduced in the MASCOT MS/MS ion search software for protein identification.

Immunoprecipitation

COS-7 cells were cotransfected with pEF-FLAG-Rab4 or pEF-FLAG-Rab5 and GRASP-1 constructs and co-immunoprecipitations were done as described [47]. Immune complexes were eluted

with FLAG peptide and analyzed by Western blot with a mouse monoclonal antibody against GFP and rabbit antibody against FLAG. For interaction studies between GRASP-1 and syntaxin 13, COS-7 cells were transfected with pGW1-GFP-GRASP-1, and pGW1-myc-syntaxin 1, pGW1-myc-syntaxin 2, or pGW1-myc-syntaxin 13. To determine the region of GRASP-1 that bound to syntaxin13, we transfected COS-7 cells with pGW1-myc-GRASP-1, pGW1-myc-GRASP-1(1–695) or pGW1-myc-GRASP-1(695–837) and pGW1-GFP-syntaxin-13. Cells were lysed in 20 mM Hepes pH 7.4, 200 mM NaCl, 1% NP-40, and protease inhibitors. Detergent lysates were passed 20× through a 27-gauge needle and centrifuged at maximum speed in a cooled Eppendorf centrifuge. The supernatant was incubated for 2 h with Rabbit GFP antibody coated beads at 4°C. Beads were washed four times with 20 mM Hepes pH 7.4, 200 mM NaCl, 1% NP-40, and immune complexes were eluted by heating for 5 min in reducing Laemmli sample buffer. Eluates were resolved by SDS-PAGE and analyzed by Western blot with monoclonal antibody against myc.

In Vitro GEF Assay

GST-Rab4, H-ras(1–166), GST-GRASP-1(1–594), and GST-cdc25(974–1260) were expressed in *E. coli* CK600K. Bacteria were grown at 37°C until OD_{600} of 0.8. IPTG was added to 1 mM and bacteria were incubated overnight at room temperature. Cells were resuspended in 50 mM Tris HCl pH 7.5, 50 mM NaCl, 5% glycerol, 5 mM DTE, and 5 mM $MgCl_2$ and lysed by sonication. Insoluble material was removed by centrifugation at 30,000 g, and in case of GST fusion proteins, the supernatant was loaded on a 20 ml GSH-column (Pharmacia). The column was washed with 5 volumes 50 mM Tris HCl pH 7.5, 400 mM NaCl, 5% glycerol 5 mM $MgCl_2$, and 5 mM DTE and 2 volumes of 50 mM Tris HCl pH 7.5, 50 mM NaCl, 2.5% glycerol 10 mM $CaCl_2$, 5 mM $MgCl_2$, and 5 mM DTE (buffer T). The proteins were cleaved with 80 units of thrombin (Serva) in buffer T on the column and elute with buffer T. Protein containing fractions were concentrated using a Millipore concentrator unit. Further purification was achieved by gel filtration on a Superdex 75 (16/60) column (Pharmacia), equilibrated with 50 mM Tris HCl pH 7.5, 50 mM NaCl, 2.5% glycerol, 5 mM $MgCl_2$, and 5 mM DTE. GTPases were loaded with 2′-(3′)-O-(N-methylanthraniloyl)-guanosinediphosphate (mantGDP) as described for rap [55]. Nucleotide exchange reactions were carried out as described [55]. In brief, 200 nM mantGDP loaded GTPase was incubated at 25°C in 50 mM Tris HCl pH 7.5, 50 mM NaCl, 5 mM $MgCl_2$, 5 mM DTE, and 5% glycerol in the presence of an 100-fold molar excess of GDP. Exchange factors were added as indicated. The fluorescence intensity was measured over time in a Cary Eclipse Spectrofluorometer (Varian), with excitation at 340 nm and emission at 460 nm.

In Vivo GEF Assay

COS-7 cells were transfected with pMT2HA-Hras together with pMT2HA-rasGRP, pGW1-myc GRASP-1, or pGW1-myc. Cells expressing HA-ras were incubated with and without 10 ng/ml EGF, and cells co-expressing HA-ras and HA-rasGRP were incubated with or without 10 μM Phorbol 12-Myristate 13-Acetate (PMA). After 5 min, the cells were lysed in 100 mM NaCl, 1% NP40, and 20 mM Hepes pH 7.5. Cleared lysates were incubated for 3 h with GSH beads containing the ras binding domain of Raf-1 [63]. Beads were washed in lysis buffer. Bound HAras-GTP and expression levels of HA-Hras, HA-rasGRP, and myc-GRASP-1 were determined by Western blot with monoclonal HA and myc antibodies, respectively.

Cultured Cells and Transfection

Hela cells and COS-7 cells were grown in DMEM containing 10% fetal calf serum, antibiotics, and 2 mM glutamine. Transferrin (Tf) uptake experiments in Hela cells were done as described [52]. INS1 cells were grown in RPMI 1640 with the same additions and 0.2 μM Na pyruvate and 50 μM β-mercaptoethanol. Cells were transfected using FuGENE6 (Roche) or Lipofectamine 2000 (Invitrogen) and used in experiments after 16–24 h. siRNAs (100 nM final concentration) were transfected with Lipofectamine 2000 in INS1 cells. After 3 d, cells were lysed and expression level of endogenous GRASP-1 was determined by Western blot.

Primary Hippocampal Neuron Cultures, Transfection, and Immunohistochemistry

Primary hippocampal cultures were prepared from embryonic day 18 (E18) rat brains [64]. Cells were plated on coverslips coated with poly-L-lysine (30 μg/ml) and laminin (2 μg/ml) at a density of 75,000/well. Hippocampal cultures were grown in Neurobasal medium (NB) supplemented with B27, 0.5 mM glutamine, 12.5 μM glutamate, and penicillin/streptomycin. Hippocampal neurons were transfected using Lipofectamine 2000 (Invitrogen). Briefly, DNA (3.6 μg/well) was mixed with 3 μl Lipofectamine 2000 in 200 μl NB, incubated for 30 min and then added to the neurons in NB at 37°C in 5% CO_2 for 45 min. Next, neurons were washed with NB and transferred in the original medium at 37°C in 5% CO_2 for 2–4 d.

For immunohistochemistry, neurons were fixed for 5 min with ice-cold 100% methanol/1mM EGTA at −20°C, followed by 5 min with 4% formaldehyde/4% sucrose in phosphate-buffered saline (PBS) at room temperature. After fixation, cells were washed three times in PBS for 30 min at room temperature and incubated with primary antibodies in GDB buffer (0.2% BSA, 0.8 M NaCl, 0.5% Triton X-100, 30 mM phosphate buffer, pH 7.4) overnight at 4°C. Neurons were then washed three times in PBS for 30 min at room temperature and incubated with Alexa-conjugated secondary antibodies in GDB for 2 h at room temperature and washed three times in PBS for 30 min. Slides were mounted using Vectashield mounting medium (Vector laboratories). Confocal images were acquired using a Zeiss LSM 510 confocal laser-scanning microscope with a 40× or 63× oil objective.

Surface and Intracellular Staining of AMPA Receptors

Surface staining of endogenous AMPARs was performed as described [10,43]. Hippocampal neurons were "live" incubated with 10 μg/ml rabbit anti-GluR1 (Calbiochem (1:8)) and mouse anti-GluR2 (Zymed (1:80)) N-terminal antibodies at 37°C for 15 min. After brief washing in prewarmed DMEM, neurons were either returned to conditioned medium (for control incubation) or stimulated for 2 min with 100 μM AMPA and 50 μM APV or 50 μM NMDA, washed in DMEM, returned to conditioned medium and incubated for the given time. The neurons were fixed for 5 min with 4% formaldehyde/4% sucrose in PBS, followed by three washes in PBS (30 min at room temperature) and incubated with secondary antibody conjugated to Alexa488 (1:400) or Alexa568 (1:400) in GDB buffer without detergent (0.2% BSA, 0.8 M NaCl, 30 mM phosphate buffer, pH 7.4) overnight at 4°C followed by a further three washes in PBS (30 min at room temperature).

The fluorescent-based AMPAR internalization assay was performed as described [10]. Hippocampal neurons transfected with HA-tagged GluR2 subunits were "live" labeled with

10 μg/ml mouse anti-HA antibody (12CA5, Roche) by incubating coverslips in conditioned medium for 10 min at 37°C. After brief washing in prewarmed DMEM, neurons were either returned to conditioned medium (for control incubation) or stimulated for 2 min with 100 μM AMPA and 50 μM APV (selective *NMDA receptor antagonist*) or 50 μM NMDA, returned to conditioned medium and incubated for the given time. Neurons were fixed in 4% formaldehyde/4% sucrose for 8 min at room temperature, and surface-remaining receptors were visualized with Alexa633-conjugated secondary antibody. Internalized receptors were detected with Alexa488-conjugated secondary antibody after permeabilizing cells in methanol (−20°C) for 2 min. To determine colocalization, the neurons were immunostained with antibodies against GRASP-1 in GDB without detergent overnight at 4°C and incubated with Alexa568-conjugated secondary antibodies for 2 h at room temperature.

The AMPAR recycling assay was performed as described [33]. After live staining for surface HA-GluR2 as indicated above, neurons were washed and either returned to conditioned medium (for control incubation) or stimulated for 2 min with 100 μM AMPA and 50 μM APV. The remaining surface anti-HA antibodies were stripped away by stripping buffer (0.5 M NaCl/0.2 M acetic acid) on ice for 4 min and washed extensively with cold TBS (Tris-buffered saline) and returned back to conditioned media at 37°C for 45 min for recycling. After recycling, neurons were fixed in 4% formaldehyde/4% sucrose, and HA-GluR2 recycled back to the surface was detected with Alexa633-conjugated secondary antibodies. Neurons were permeabilized, and internal HA-GluR2 was detected with Alexa568-conjugated secondary antibodies.

Immunohistochemistry and Confocal Immunofluorescence

The mouse spinal cord was sectioned at 40 μm with a freezing microtome. Sections were processed free floating, employing double-labeling immunofluorescence [65]. The antibodies were diluted in Tris-Buffered-Saline (TBS, pH7.6) containing 1% normal horse serum and 0.2% Triton X-100. Sections stained for immunofluorescence were analyzed with a Zeiss LSM 510 confocal laser-scanning microscope.

Time-Lapse Live Cell Imaging

During imaging, neurons were maintained at 37°C in standard culture medium in a closed chamber with 5% CO2 (Tokai Hit; INUG2-ZILCS-H2). To visualize mRFP-GRASP-1 and GFP-Rab4 or mRFP-GRASP-1 and GFP-Rab11 in neurons, near-simultaneous dual color (green and red) time-lapse live cell imaging was performed using Total Internal Reflection Fluorescence microscopy (TIRFM) on a Nikon Eclipse TE2000E (Nikon), equipped with Nikon TIRF arm, CFI Apo TIRF 100×1.49 N.A. oil objective (Nikon), Coolsnap camera (Roper Scientific), and controlled by MetaMorph 7.1 software (Molecular Devices). For excitation, the 488 nm laser line of an argon laser (Spectra-Physics Lasers) and a 561 nm laser (Spectra-Physics) were used in combination with a ETGFP/mCherry filter cube (Chroma). A filterwheel (Sutter instruments) with GFP and Cherry emission filters (both Chroma) and synchronized with laser emission alternatingly exposed the camera to GFP or Cherry emission. For glycine treatments, the same microscope was used with regular widefield illumination by a mercury lamp. Glycine treatments were performed as described in [2]. Images of live cells were processed and analyzed using MetaMorph, Adobe Photoshop, or LabVIEW (National Instruments) software.

Image Analysis and Quantification

Confocal images of transfected neurons were obtained with sequential acquisition settings at the maximal resolution of the microscope (1,024×1,024 pixels). Each image was a z-series of 6–8 images, each averaged 2 times and was chosen to cover the entire region of interested from top to bottom. The resulting z-stack was "flattened" into a single image using maximum projection. Images were not further processed and were of similar high quality to the original single planes. The confocal settings were kept the same for all scans when fluorescence intensity was compared. Morphometric analysis, quantification, and colocalization were performed using MetaMorph software (Universal Imaging Corporation).

Morphometric analyses of hippocampal neurons. To visualize the dendritic protrusions, we used β-gal or GFP as an unbiased cell-fill. Because protrusions often crossed several z planes, we took series of stacks from the bottom to the top of all dendrites and used the LSM software to generate image projections for quantitative analyses. All morphological experiments were repeated at least three times with an $n>7$ for individual experiments and were analyzed in a double-blind manner. Between 150 and 300 protrusions were scored for every neuron and expressed per 10 μm length of dendrite. Measurements of length and width of the protrusions were performed as described previously [66] and were classified based on the ratio of spine head width to protrusion length according to the following ratios: the spine whose width was equal to or more than half the size of its length was judged as standard mushroom spine. The protrusion whose width was smaller than half the size of its length was judged as filopodia or thin spine. In those cases where the total length of the spine could not be adequately seen or its length was >5 μm, protrusions were excluded from analysis.

Quantification of TfR-GFP distribution in spines. Measurements of TfR-GFP localization in spines and dendrites was performed as described [2]. Confocal images of hippocampal neurons filled with β-gal (red) and labeled for TfR-GFP were analyzed using Metamorph software. The dendritic localization of TfR positive structures relative to spines was categorized according to the presence of GFP signal at the base (a), in the neck (b), or in the head (c) of spines.

Colocalization of fluorescent signals in dendrites and cell body. Colocalization of two fluorescent signals was determined using "colocalization" module in Metamorph software as described [10]. The colocalization module provides intensity measurements of the region overlap between signals in red and green channels of image projections. To minimize random overlap due to projection of confocal images, a single optical section from the z series stack that showed the largest amount of fluorescent signals was used to determine the degree of colocalization in the cell body. Statistical analysis was performed with Student's t test assuming two-tailed distribution and unequal variation. n was defined as the number of transfected cells.

Quantification of surface and internalized AMPARs. To measure AMPAR internalization and recycling, images for all conditions in individual experiments were analyzed by using identical microscope settings. Images from each experiment were thresholded, and total staining intensity of surface and internalized GluR1 and/or GluR2 was measured along selected dendritic areas using Metamorph. The internalization index refers to intracellular fluorescence divided by surface fluorescence normalized to untreated control neurons. For experiments comparing internalized and surface staining of AMPARs, dendritic areas were manually drawn and staining intensity in the same selected area was measured in the different channels. The recycling index was calculated as the ratio of surface fluorescence divided by the

internalized fluorescence and normalized to unstimulated wild-type control neurons.

Analysis of morphological changes upon glycine treatment. For each protrusion, length and maximum width were measured in MetaMorph. Only protrusions longer than 7 pixels (450 nm) were included in the analysis. Protrusions were identified as spines if their width was greater than half their length or greater than 10 pixels (645 nm). Spine growth was probed as the change in sum of spine widths per 10 um and comprises both addition of new spines and growth of pre-existing spines.

Immuno Electronmicroscopy

Hippocampal neurons (DIV>21) were fixed in paraformaldehyde or a mixture of paraformaldehyde/glutaraldehyde and processed for immunoelectronmicroscopy on ultrathin cryosections as described [67]. Sections were labeled with mouse monoclonal antibody against rab4, and rabbit antibodies against syntaxin 13 [35], or GRASP-1 (#5285).

Electrophysiology

Electrophysiological recordings were carried out from organotypic slice cultures as described [68]. Neurons were transfected using a biolistic gene gun (Bio Rad) at DIV 3–4 (100 µg DNA; 90% of the construct to test; 10% pCAG-EGFP). Electrophysiological recordings were performed at 5–6 d after transfection. Recordings were carried out in solution containing NaCl, 119 (mM); KCl, 2.5; $CaCl_2$, 4; $MgCl_2$, 4; $NaHCO_3$, 26; NaH_2PO4, 1; glucose, 11; picrotoxin, 0.15; and 2-chloroadenosine, 0.01 for measuring AMPAR- and NMDAR-EPSC and 0.002 for LTP experiments with 5% CO_2/95% O_2, at pH7.4. Whole-cell recordings were made simultaneously from a pair of CA1 pyramidal neurons, one transfected and one untransfected, and synaptic responses were evoked by tungsten bipolar electrode placed in CA1 stratum radiatum area with the frequency of 0.2 Hz. AMPAR-mediated EPSCs were measured at −60 mV and NMDAR-EPSCs were recorded at −40 mV in the presence of NBQX (0.01 mM). AMPAR-EPSCs for LTP experiment were measured at −80 mV and LTP was induced by pairing 2 Hz stimulation with depolarization of the postsynaptic cell to 0 mV for 100 s. Statistical significance was evaluated with the Mann-Whitney test (Figure 5A,B) and *t* test (Figure 5C,D).

Supporting Information

Figure S1 Localization of Rab4 and GRASP in vivo. Mouse spinal cord sections of 40 µm were double-labeled for endogenous GRASP-1 (green) and Rab4 (red). Sections were examined on a Zeiss LSM510 at low magnification to obtain the overview image (top row) or high magnification (bottom row). Arrowheads denote colocalization between GRASP-1 and Rab4 as also shown in the inset with merged colors.
Found at: doi:10.1371/journal.pbio.1000283.s001 (3.04 MB TIF)

Figure S2 Rab4 dominant negative mutant affects GRASP-1 localization. (A–C) Representative images of hippocampal neurons transfected with GDP-bound dominant negative mutant GFP-Rab4S22N at DIV13 for 2 d and stained for endogenous GRASP-1 (A), syntaxin 13 (B), or Neep21 (C). Note that in the neurons transfected with Rab4S22N, almost no GRASP-1 puncta are present in somatodendritic compartments while the localization of syntaxin 13 and Neep21 is unchanged. Arrows indicate transfected neurons in the red channel. Bar is 10 µm. (D–F) Quantification of GRASP-1 fluorescence intensities in cell body of hippocampal neurons transfected as indicated in (A–C). Graphs show mean ± SEM normalized to neighboring neurons. *** $p<0.0005$.
Found at: doi:10.1371/journal.pbio.1000283.s002 (3.54 MB TIF)

Figure S3 GRASP-1 shRNA suppresses expression of GRASP-1. (A) Representative images of hippocampal neurons cotransfected at DIV13 with GFP and either pSuper, pSuper-GRASP-1-shRNA#2, or -shRNA#5 and visualized after 4 d with rabbit antibody against GRASP-1 (red) and GFP (green). Cell body (inset) is enlarged to show loss of GRASP-1 immunoreactivity in GRASP-1-shRNA transfected neurons. Bar is 10 µm. (B) Quantification of GRASP-1 fluorescence intensities in cell body and dendrites of hippocampal neurons transfected at DIV13 for 4 d with GFP and either pSuper, pSuper-GRASP-1-shRNA#2, or -shRNA#5. Staining was done with two distinct rabbit anti-GRASP-1 antibodies: clone JH 2730 and AB96361. Graph shows mean ± SEM normalized to pSuper control neurons. *** $p<0.0005$. (C) Western blot of lysates prepared from INS-1 cells transfected with 100 nM (final concentration) of three siRNAs (Ambion), a smartpool (Dharmacon), or control scrambled siRNA (Dharmacon) for 3 d. siRNA#2 and the smartpool reduced GRASP-1 expression to 15% and 23%, respectively. We cloned the siRNA#2 sequence in pSuper in order to generate pSuper-GRASP-1-shRNA#2 (A,B).
Found at: doi:10.1371/journal.pbio.1000283.s003 (3.01 MB TIF)

Figure S4 Internalized HA-GluR2 colocalizes with GRASP-1. (A) Representative merge image of surface HA-GluR2 (blue) and internalized HA-GluR2 (green) in soma and dendrites of hippocampal neurons labeled for GRASP-1 (red) after 0, 10, and 30 min 100 µM AMPA plus 50 µM APV (AMPA) stimulation. (B) Quantification of the percentage of colocalization of internalized GluR2 with GRASP1 after AMPA/APV treatment at different time points. Each data point represents mean±S.E.M. (5 neurons for each time point). (C) Representative images of neurons triple transfected at DIV13 with GFP and HA-GluR2 and either pSuper control vector or pSuper-GRASP-1-shRNA#2. After 4 d, neurons are "live" labeled with anti-HA antibody for 15 min, followed by 10 min incubation in conditioned medium (control, no treatment) or 2 min incubation in conditioned medium containing 100 µM AMPA plus 50 µM APV (AMPA) followed by additional 8 min in conditioned medium. The neurons are stained for surface and internalized HA-GluR2. (D) Quantification of intracellular accumulation assays, measured as the ratio of internalized/surface fluorescence (internalization index), normalized to GluR2 10 min control (no treatment). Graph shows mean ± S.E.M. (10 neurons for each condition). (E) Representative merge images of neurons cotransfected at DIV13 with HA-GluR2 and either pSuper control vector or pSuper-GRASP-1-shRNA#2 and stained for internalized HA-GluR2 (red) and lysosomal marker Lamp1 (green) in the cell body after stimulation for 30 min with AMPA. (F) Quantification of the percentage of colocalization of internalized GluR2 with Lamp1 as indicated in (E). Graph shows mean ± S.E.M. (5 neurons each). ** $p<0.005$.
Found at: doi:10.1371/journal.pbio.1000283.s004 (2.15 MB TIF)

Figure S5 GRASP-1 colocalizes with Rab4 and Rab11 in Hela cells. (A) Hela cells co-transfected with myc-GRASP-1 and GFP-Rab4, GFP-Rab5, GFP-Rab7, or GFP-Rab11. Bar is 10 µm. (B) Percentage of colocalization between GRASP-1 and Rab proteins in Hela cells as indicated in (A).
Found at: doi:10.1371/journal.pbio.1000283.s005 (2.99 MB TIF)

Figure S6 GRASP-1 colocalizes with endogenous recycling endosome markers. Representative images of cell bodies

of hippocampal neurons transfected with GFP-GRASP-1 and labeled with anti-Rab4, anti-Rab5, anti-Rab11, anti-NEEP21, or anti-syntaxin 13 antibodies (all red).
Found at: doi:10.1371/journal.pbio.1000283.s006 (2.27 MB DOC)

Figure S7 GRASP-1 regulates EEA1 distribution in Hela cells. (A) Percentage of colocalization between EEA1 and Rab4 or Rab5 in Hela cells with and without transfected myc-GRASP-1 as shown in (C,D). Error bars indicate S.E.M. *** $p<0.0005$. (B) Hela cells transfected with myc-GRASP-1 and double labeled with anti-EEA1 (red) and anti-myc (green) antibodies. Note the lack of colocalization between EEA1 and GRASP1. Bar is 10 μm. (C–D) Hela cells co-transfected with GFP-Rab4 (C) or GFP-Rab5 (D) with and without myc-GRASP-1. Cells were labeled with anti-EEA1 (red) and anti-myc (blue) antibodies. Bar is 10 μm.
Found at: doi:10.1371/journal.pbio.1000283.s007 (2.50 MB TIF)

Figure S8 GRASP-1 segregates Rab4 from NEEP21 positive endosomal membranes. (A) Representative images of hippocampal neurons double labeled with anti-EEA1 (green) and anti-NEEP21 (red) antibodies. Dendritic segments are enlarged to show the distribution of the markers (bottom). (B,C) Representative images of dendrites of hippocampal neurons cotransfected at DIV13 for 4 d with GFP-Rab5 (B) or GFP-TfR (C) and labeled with anti-NEEP21 (red). (D) Representative images of dendrites of hippocampal neurons cotransfected at DIV13 for 4 d with GFP-Rab4 and pSuper control vector, myc-GRASP-1, or pSuper-GRASP-1-shRNA#2 and labeled with anti-NEEP21 (red) and anti-myc (blue) antibodies.
Found at: doi:10.1371/journal.pbio.1000283.s008 (1.30 MB TIF)

Figure S9 GRASP-1 coincides with Rab4 and syntaxin 13 in Hela cells. (A) Hela cells co-transfected with GFP-GRASP-1 and myc-syntaxin 1, myc-syntaxin 2, or myc-syntaxin 13. (B) Hela cells triple transfected with GFP-GRASP-1, myc-syntaxin 13, and HA-Rab4. Bar is 10 μm.
Found at: doi:10.1371/journal.pbio.1000283.s009 (3.70 MB DOC)

Figure S10 Both N and C terminus are necessary for GRASP-1 localization to endosomes. Hela cells transfected with full-length mRFP-GRASP-1 (1–837) or truncated mRFP-GRASP-1 constructs and labeled with anti-TfR antibodies (green). Bar is 10 μm.
Found at: doi:10.1371/journal.pbio.1000283.s010 (5.64 MB TIF)

Video S1 GFP-Rab4 (left) and mRFP-GRASP-1 (right) in hippocampal neurons visualized using TIRF. This video corresponds to Figure 2G. Total time 3 min. Acquired at 0.5 frame per second. 30× sped up.
Found at: doi:10.1371/journal.pbio.1000283.s011 (3.88 MB AVI)

Video S2 GFP-Rab4 (left) and mRFP-GRASP-1 (middle) in hippocampal neurons visualized using TIRF. This video corresponds to Figure 2G. Right movie shows GFP and RFP in green and red, respectively. Total time 3 min. Acquired at 0.5 frame per second. 30× sped up.
Found at: doi:10.1371/journal.pbio.1000283.s012 (1.70 MB AVI)

Video S3 GFP-Rab11 (left) and mRFP-GRASP-1 (right) in hippocampal neurons visualized using TIRF. This video corresponds to Figure 7B. Total time 3:22 (min:s). Acquired at 1 frame per second. 30× sped up.
Found at: doi:10.1371/journal.pbio.1000283.s013 (5.52 MB AVI)

Video S4 GFP-Rab11 (left) and mRFP-GRASP1 (middle) in hippocampal neurons visualized using TIRF. This video corresponds to Figure 7B. Right movie shows GFP and RFP in green and red, respectively. Total time 3:22 (min:s). Acquired at 1 frame per second. 30× sped up.
Found at: doi:10.1371/journal.pbio.1000283.s014 (1.01 MB AVI)

Acknowledgments

We thank Dr. Richard Huganir for GRASP-1 antibody and constructs, Dr. Harald Hirling for Neep21 antibody and Neep21 and syntaxin 13 constructs, Dr. Gary Banker for TfR constructs, Dr. Mitsunori Fukuda for Flag-Rab4 and Flag-Rab5, Samantha Spangler and Nanda Keijzer for preparing primary hippocampal neuronal cultures, Mathijs Vleugel and Bianka Martini for technical assistance, and René Scriwanek and Marc van Peski for preparing the EM figure.

Author Contributions

The author(s) have made the following declarations about their contributions: Conceived and designed the experiments: CCH PvdS. Performed the experiments: CCH IP KF ESM PSW TvV BRD VO MM HR DJ LCK PvdS. Analyzed the data: CCH IP KF BRD LCK PvdS. Contributed reagents/materials/analysis tools: RG AJRH MS JK. Wrote the paper: CCH PvdS.

References

1. Sheng M, Hoogenraad CC (2007) The postsynaptic architecture of excitatory synapses: a more quantitative view. Annu Rev Biochem 76: 823–847.
2. Park M, Salgado JM, Ostroff L, Helton TD, Robinson CG, et al. (2006) Plasticity induced growth of dendritic spines by exocytic trafficking from recycling endosomes. Neuron 52: 817–830.
3. Maxfield FR, McGraw TEM (2004) Endocytic recycling. Nature Rev Mol Cell Biol 5: 121–132.
4. Gould GW, Lippincott-Schwartz JL (2009) New roles for endosomes: from vesicular carriers to multipurpose platforms. Nature Rev Mol Cell Biol 11: 287–292.
5. Bredt DS, Nicoll RA (2003) AMPA receptor trafficking at excitatory synapses. Neuron 40: 361–379.
6. Malinow R, Malenka RC (2002) AMPA receptor trafficking and synaptic plasticity. Annu Rev Neurosci 25: 103–126.
7. Barry MF, Ziff EB (2002) Receptor trafficking and the plasticity of excitatory synapses. Curr Opin Neurobiol 12: 279–286.
8. Shepherd JD, Huganir RL (2007) The cell biology of synaptic plasticity: AMPA receptor trafficking. Annu Rev Cell Biol Dev Biol 23: 613–643.
9. Ehlers MD (2000) Reinsertion or degradation of AMPA receptors determined by activity-dependent endocytic sorting. Neuron 28: 511–525.
10. Lee SH, Simonetta A, Sheng M (2004) Subunit rules governing the sorting of internalized AMPA receptors in hippocampal neurons. Neuron 43: 221–336.
11. Gruenberg J (2001) The endocytic pathway: a mosaic of domains. Nature Rev Mol Cell Biol 2: 721–730.
12. Park M, Pencik EC, Edwards JG, Kauer JA, Ehlers MD (2004) Recycling endosomes supply AMPA receptors for LTP. Science 305: 1972–1975.
13. Steiner P, Sarria JCF, Glauser L, Magnin S, Catsicas S, et al. (2002) Modulation of receptor recycling by neuron-enriched endosomal protein of 21 kDa. J Cell Biol 157: 1197–1209.
14. Cai H, Reinisch K, Ferro-Novick S (2007) Coats, tethers, Rabs, and SNAREs work together to mediate the intracellular destination of a transport vesicle. Dev Cell 12: 671–682.
15. Zerial M, McBride H (2001) Rab proteins as membrane organizers. Nature Rev Mol Cell Biol 2: 107–117.
16. Deneka M, Neeft M, van der Sluijs P (2003) Rab GTPase switch in membrane dynamics. CRC Rev Biochem Mol Biol 38: 121–142.
17. Murthy VN, de Camilli P (2003) Cell biology of the presynaptic terminal. Annu Rev Neurosci 26: 701–728.
18. Sudhof TC (2004) The synaptic vesicle cycle. Annu Rev Neurosci 27: 509–547.
19. Kennedy MJ, Ehlers MD (2006) Organelles and trafficking machinery for postsynaptic plasticity. Annu Rev Neurosci 29: 325–362.
20. Greger IH, Esteban JA (2007) AMPA receptor biogenesis and trafficking. Curr Opin Neurobiol 17: 289–297.
21. Brown TC, Tran IC, Backos DS, Esteban JA (2005) NMDA receptor dependentactivation of the small GTPase rab5 drives the removal of synaptic AMPA receptors during hippocampal LTD. Neuron 45: 81–94.

22. Brown TC, Correia SS, Petrok CN, Esteban JA (2007) Functional compartmentalization of endosomal trafficking for the synaptic delivery of AMPA receptors during long term potentiation. J Neurosci 27: 13311–13315.
23. Gerges NZ, Backos DS, Esteban JA (2004) Local control of AMPA receptor trafficking at the postsynaptic terminal by a small GTPase of the rab family. J Biol Chem 279: 43870–43878.
24. Sönnichsen B, de Renzis S, Nielsen E, Rietdorf J, Zerial M (2000) Distinct membrane domains on endosomes in the recycling pathway visualized by multicolor imaging of rab4, rab5, and rab11. J Cell Biol 149: 901–913.
25. de Renzis S, Sönnichsen B, Zerial M (2002) Divalent rab effectors regulate the sub-compartmental organization and sorting function of early endosomes. Nature Cell Biol 4: 124–133.
26. Deneka M, van der Sluijs P (2002) 'Rab'ing up endosomal membrane transport. Nature Cell Biol 4: E33–E35.
27. van der Sluijs P, Hull M, Webster P, Goud B, Mellman I (1992) The small GTP binding protein rab4 controls an early sorting event on the endocytic pathway. Cell 70: 729–740.
28. Ye B, Liao D, Zhang X, Zhang P, Dong H, et al. (2000) GRASP-1: a neuronal rasGEF associated with the AMPA receptor/GRIP complex. Neuron 26: 603–617.
29. Vitale G, Rybin V, Christoforidis S, Thornqvist PO, McCaffrey M, et al. (1998) Distinct rab-binding domains mediate the interaction of rabaptin-5 with GTP-bound rab4 and rab5. EMBO J 17: 1941–1951.
30. Ye B, Yu WP, Thomas GM, Huganir RL (2007) GRASP-1 is a neuronal scaffold protein for the JNK signaling pathway. FEBS lett 581: 4403–4410.
31. Stinton LM, Selak S, Fritzler MJ (2005) Identification of GRASP-1 as a novel 97 kDa autoantigen localized to endosomes. Clin Immunol 116: 108–117.
32. Ebinu JO, Bottorf DA, Chan EY, Stang SL, Dunn RJ, et al. (1998) RasGRP, a ras guanyl nucleotide-releasing protein with calcium and diacylglycerol binding. Science 280: 1082–1086.
33. Lu W, Ziff EB (2005) PICK1 interacts with ABP/GRIP to regulate AMPA receptor trafficking. Neuron 47: 407–421.
34. Trischler M, Stoorvogel W, Ullrich O (1999) Biochemical analysis of distinct rab5- and rab11 positive endosomes along the transferrin pathway. J Cell Sci 112: 4773–4783.
35. Prekeris R, Klumperman J, Chen YA, Scheller RH (1998) Syntaxin 13 mediates cycling of plasma membrane proteins via tubulovesicular recycling endosomes. J Cell Biol 143: 957–971.
36. McBride HM, Rybin V, Murphy C, Giner A, Teasdale R, et al. (1999) Oligomeric complexes link rab5 effectors with NSF and drive membrane fusion via interactions between EEA1 and syntaxin 13. Cell 98: 377–386.
37. Stenmark H (2009) Rab GTPases as coordinators of vesicle traffic. Nature Rev Mol Cell Biol 10: 513–525.
38. Bonifacino JS, Rojas R (2006) Retrogade transport from endosomes to the trans Golgi network. Nature Rev Mol Cell Biol 7: 568–579.
39. Zwilling D, Cypionka A, Pohl WA, Fasshauer D, Walla PJ, et al. (2007) Early endosomal SNAREs form a structurally conserved SNARE complex and fuse liposomes with multiple topologies. EMBO J 26: 9–18.
40. Ohya T, Miaczynska M, Coskun U, Lommer B, Runge A, et al. (2009) Reconstitution of rab and SNARE dependent membrane fusion by synthetic endosomes. Nature 459: 1091–1097.
41. Grosshans BL, Ortiz D, Novick P (2006) Rabs and their effectors: achieving specificity in membrane transport. Proc Natl Acad Sci U S A 103: 11821–118827.
42. Wang Z, Edwards JG, Provance DW, Karcher R, Lim XD, et al. (2008) Myosin Vb mobilizes recycling endosomes and AMPA receptors for postsynaptic plasticity. Cell 135: 535–548.
43. Hoogenraad CC, Milstein AD, Ethell IM, Henkemeyer M, Sheng M (2005) GRIP1 controls dendrite morphogenesis by regulating EphB receptor trafficking. Nature Neurosci 8: 906–915.
44. Steiner P, Alberi S, Kulangara K, Yersin A, Sarria JC, et al. (2005) Interactions between NEEP21, GRIP1 and GluR2 regulate sorting and recycling of the glutamate receptor subunit GluR2. EMBO J 24: 2873–2884.
45. Kulangara K, Kropf M, Glauser L, Magnin S, Alberi S, et al. (2007) Phosphorylation of Glutamate receptor interacting protein 1 regulates surface expression of Glutamate receptors. J Biol Chem 282: 2395–2404.
46. Jaworski J, Kapitein LC, Gouveia SM, Dortland BR, Wulf PS, et al. (2009) Dynamic microtubules regulate spine morphology and synaptic plasticity. Neuron 61: 85–100.
47. van Vlijmen T, Vleugel M, Evers M, Mohammed S, Wulf PS, et al. (2008) A unique residue in rab3c determines the interaction with novel binding protein Zwint-1. FEBS lett 582: 2938–2942.
48. Fukuda M (2003) Distinct rab binding specificity of rim1, rim2, rabphilin, and noc2. J Biol Chem 278: 15373–15380.
49. Jordens I, Fernandez-Borja M, Marsman M, Dusseljee S, Janssen H, et al. (2001) The rab7 effector protein RILP controls lysosomal transport by inducing the recruitment of dynein-dynactin motors. Curr Biol 11: 1680–1685.
50. Burack MA, Silverman MA, Banker G (2000) The role of selective transport in neuronal protein sorting. Neuron 26: 465–472.
51. Roberts M, Barry S, Woods A, van der Sluijs P, Norman J (2001) Rab4-dependent recycling of avb3 integrin from early endosomes is necessary for cell adhesion and spreading. Curr Biol 11: 1392–1402.
52. Deneka M, Neeft M, Popa I, van Oort M, Sprong H, et al. (2003) Rabaptin-5a/rabaptin-4 serves as a linker between rab4 and g1-adaptin in membrane recycling from endosomes. EMBO J 22: 2645–2657.
53. de Graaf P, Zwart WT, van Dijken RAJ, Deneka M, Schulz T, et al. (2004) Phosphatidylinositol 4-kinaseb is critical for functional association of rab11 with the Golgi complex. Mol Biol Cell 15: 2038–2047.
54. Cormont M, Mari M, Galmiche A, Hofman P, Le Marchand Brustel Y (2001) A FYVE finger-containing protein, rabip4, is a rab4 effector protein involved in early endosomal traffic. Proc Natl Acad Sci U S A 98: 1637–1642.
55. Rehmann H (2005) Characterization and activation of the rab-specific exchange factor Epac by cyclic nucleotides. Meth Enzymol 407: 159–173.
56. Wilcke M, Johannes L, Galli T, Mayou V, Goud B, et al. (2000) Rab11 regulates the compartmentalization of early endosomes required for efficient transport from early endosomes to the trans Golgi network. J Cell Biol 151: 1207–1220.
57. de Wit H, Liechtenstein Y, Kelly RB, Geuze HJ, Klumperman J, et al. (2001) Rab4 regulates formation of synaptic-like microvesicles from early endosomes in PC12 cells. Mol Biol Cell 12: 3703–3715.
58. Brummelkamp TR, Bernards R, Agami R (2002) A system for stable expression of short interfering RNAs in mammalian cells. Science 296: 550–553.
59. Yuan B, Latek R, Hossbach M, Tuschl T, Lewitter F (2004) siRNA selection server: an automated siRNA oligonucleotide prediction server. Nucl Acid Res 32: W130–W134.
60. Zhang H, Macara IG (2006) The polarity protein PAR-3 and TIAM1 cooperate in dendritic spine morphogenesis. Nature Cell Biol 8: 227–237.
61. Neeft M, Wieffer M, de Jong AS, Negroiu G, Metz CH, et al. (2005) Munc13-4 is and effector of rab27a and controls secretion of lysosomes in haematopoietic cells. Mol Biol Cell 16: 731–741.
62. Gerez L, Mohrmann K, van Raak M, Jongeneelen M, Zhou XZ, et al. (2000) Accumulation of rab4 GTP in the cytoplasm and association with the peptidyl-prolyl isomerase Pin1 during mitosis. Mol Biol Cell 11: 2201–2211.
63. de Rooij J, Bos JL (1997) Minimal ras-binding domain of raf1 can be used as an activation probe for ras. Oncogene 14: 623–625.
64. Goslin K, Banker G (1990) Rapid changes in the distribution of GAP-43 correlate with the expression of neuronal polarity during normal development and under experimental conditions. J Cell Biol 110: 1319–1331.
65. Jaarsma D, Rognoni F, van Duijn W, Verspaget H, Haasdijk ED, et al. (2001) CuZn superoxide dismutase (SOD1) accumulates in vacuolated mitochondria in transgenic mice expressing amyotrophic lateral sclerosis-linked SOD1 mutations. Acta Neuropathol 102: 293–305.
66. Jaworski J, Kapitein LC, Gouveia SM, Dortland BR, Wulf PS, et al. (2009) Dynamic microtubules regulate spine morphology and synaptic plasticity. Neuron 61: 85–100.
67. Slot JW, Geuze HJ (2007) Cryosectioning and immunolabeling. Nature Protoc 2: 2480–2491.
68. Futai K, Kim MJ, Hashikawa T, Scheifele P, Sheng M, et al. (2007) Retrograde modulation of presynaptic release probability through signaling mediated by PSD-95-neuroligin. Nature Neurosci 10: 186–195.